PAPER

Dispenser printing of piezo-resistive nanocomposite on woven elastic fabric and hysteresis compensation for skin-mountable stretch sensing

IOP Publishing Smart Materials and Structures
Smart Mater. Struct. 27 (2018) 025017 (16pp) https://doi.org/10.1088/1361-665X/aaa5e3

Dispenser printing of piezo-resistive nanocomposite on woven elastic fabric and hysteresis compensation for skin-mountable stretch sensing

Hyosang Lee[1,5], Haedo Cho[2,5], Sangjoon J Kim[3], Yeongjin Kim[4] and Jung Kim[3,6]

[1] Max-Planck-Institute for Intelligent Systems, Heisenbergstr. 3 70569, Stuttgart, Germany
[2] Beflex Inc., Changjo B/D,193 Munji-ro, Yuseong-gu, Daejeon 34051, Republic of Korea
[3] Korea Advanced Institute of Science and Technology, 291 Daehak-ro, Yuseong-gu, Daejeon 34141, Republic of Korea
[4] Incheon national university, 119 Academy-ro, Yeonsu-gu, Incheon, 22012, Republic of Korea

E-mail: hslee@is.mpg.de, johnc@beflex.co, kim6224kr@gmail.com, sangjoon.j.kim@kaist.ac.kr and jungkim@kaist.ac.kr

Received 6 November 2017, revised 27 December 2017
Accepted for publication 8 January 2018
Published 24 January 2018

Abstract

Recently, piezo-resistive nanocomposites have emerged as an important smart material for realizing less obtrusive and more comfortable stretch sensing applications. To manufacture cost-effective and skin-mountable stretch sensor, dispenser printing is advantageous method because piezo-resistive nanocomposites can be directly printed on a woven elastic fabric in various patterns. However, both electrical and mechanical properties of the nanocomposites need to be modulated to achieve favorable sensing performance as well as strong adhesion between the nanocomposite and the fabric to sustain large strains. Moreover, inherent hysteretic behavior of the soft nanocomposite should be compensated to obtain consistent stretch sensing. This paper presents silicone rubber mixed with long multi-walled carbon nanotubes (Long-MWCNTs) composites as a piezo-resistive transducing material for dispenser printing. High aspect ratio of the Long-MWCNTs resulted in low viscosity of a liquid state nanocomposite and high electrical conductivity. Due to the low viscosity, the liquid state nanocomposite could permeate into gaps of the woven elastic fabrics and ensured strong bonding force in large strains up to 35%. In addition, a modified Prandtl-Ishilinskii (MPI) model was adopted to compensate for piezo-resistive hysteresis of the nanocomposite. For validation, the skin-mountable sensor was applied to estimate rotation angle of a wrist. The sensor system estimated the rotation angle of the wrist with an estimation error of 1.93 degrees within 65 degrees range (2.9%) for the step increment and decrement test, and 7.15 degrees within 75 degrees range (9.5%) for the arbitrary movement test. Thus, the experimental results show that the dispenser printing method incorporated with hysteresis compensation can provide a guideline to implement skin-mountable smart fabrics for stretch sensing using various nanocomposites

Supplementary material for this article is available online

[5] These authors contributed equally to this work.
[6] Author to whom any correspondence should be addressed.

Keywords: piezo-resistive nanocomposite, dispenser printing, hysteresis compensation, skin-mountable stretch sensing

(Some figures may appear in colour only in the online journal)

1. Introduction

Piezo-resistive nanocomposites have risen as a prominent smart material for biomedical research, rehabilitation robots and entertainment because of its stretchability and manufacturability for a user specific design in wearable motion sensing applications [1–3]. Conventionally, inertial measurement units (IMUs) [4] or magnetic field sensors [5] have been widely adopted as a gold standard in wearable motion sensing, but such sensors have several limitations for instance, limited work space in case of the magnetic field sensors, high cost and low wearability for both systems. The progress in soft materials and electronics have enabled conformable motion sensing methods utilizing stretch of liquid-metals [6], metal-coated fabrics [7, 8], parallel dielectric layers [9], and optical components [10, 11]. Among these methods, piezo-resistive nanocomposites have major advantages in wearable motion sensing applications because the nanocomposites can be integrated to simple and cost-effective fabrication processes including dispenser printing, screen printing, and 3D printing techniques [1, 12].

Dispenser printing is a direct-write process that nanocomposites are directly deposited on a substrate without the need for expensive tooling or lithographic masks [1, 13]. This method is beneficial for wearable applications because customization of printing patterns for the user can be simply achieved. For this reason, dispenser printing has been utilized to various applications including flexible batteries [14, 15] and wearable electronics [12]. To apply dispenser printing, both the properties of the printing material and the printing parameters were tightly controlled to achieve optimized performance. A selection of proper substrate is also important for dispenser printing. Considering stretchable and breathable characteristics in wearable motion sensing application, woven elastic fabric is a preferable substrate [16]. Numerous studies have been conducted to fabrics as a printing substrate due to its wide range of applications [17–21]. To apply dispenser printing to fabrics, surface uniformity and porosity of the fabric were investigated and improved through an interface layer between the fabric and the printing material [17, 18].

Recently, many wearable human motion sensing methods have been demonstrated using highly conformable piezo-resistive nanocomposites. However, most of the previous systems needed inextensible straps or sleeves to fix the sensors to the wearer's skin [22–25]. These additional devices interrupt the natural motion of the wearer and produce discomfort, especially in the case of long-term usages. In contrast, skin-mountable stretch sensing method could offer a simple and inconspicuous motion sensing system without any excessive devices for daily motion monitoring and classification [13, 26, 27]. To achieve low fabrication cost and facile customization in skin-mountable stretch sensing, dispenser printing have been applied using nanocomposite with elastic fabrics [28–30]. Although previous approaches showed moderate performances, still two issues need to be resolved for practical applications.

A challenging issue is maintaining adhesion between the nanocomposites and the woven elastic fabric while providing stretch sensing performance near 30% strain. These two distinct materials can be separated if large shear stress occurs along the contact surfaces due to the difference in the elastic modulus of the adjacent materials. To prevent detachment, both materials should be compliant enough to prevent mechanical failure under high strain conditions, and a certain amount of adhesion force should be obtained. To ensure compliance, polymeric elastomers are widely used as a bulk matrix for synthesis of the nanocomposite [31]. Conductive nanomaterials such as carbon nanotubes (CNT) [31–34], metal nanoparticles [35], and silver nanowires [36] can be mixed with the elastomers to acquire piezo-resistive characteristics. Regarding the adhesion between two distinct materials, strong adhesion force can be achieved through modulating mechanical characteristics of the materials [37]. A simple and effective approach to obtain strong adhesive force can be utilizing a woven structure of the elastic fabric and fluidic characteristic of the uncured state of nanocomposite. To obtain strong adhesion force, the contact surfaces between two materials can be increased through permeating the uncured state nanocomposite into gaps of the woven structures. The stretch sensing performances including sensitivity, linearity, hysteresis as well as the mechanical properties of the nanocomposite depend on the selection of the materials and synthesis process. For this reason, optimized nanocomposite is required for the skin-mountable stretch sensing application.

Another issue is compensating piezo-resistive hysteresis of the nanocomposites which is known for a major drawbacks of resistance-type sensors [1, 2]. Friction force between nanomaterials and the inherent viscoelasticity of the nanocomposite are regarded as the main causes of this undesirable behavior [38, 39]. These factors affect the formation and destruction of conductive pathways constituted by conductive nanomaterials. Many approaches have been introduced to reduce the impacts of these factors through structural modification [40] or filler concentration optimization [39]. However, the correction of nonlinear hysteresis using mathematical modeling is unavoidable to improve the stretch sensing accuracy. Few studies were conducted to compensate piezo-resistive hysteresis. For pressure sensing application, Duhem hysteresis model was applied to the CNT/PDMS nanocomposite [41]. This model could compensate frequency dependent hysteresis behavior. In case of the frequency

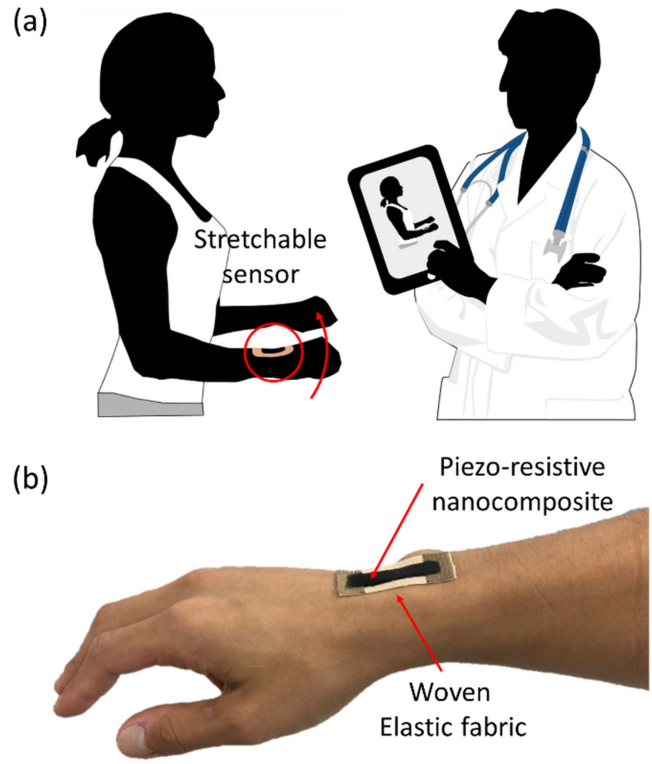

Figure 1. (a) Concept of the skin-mountable motion monitoring system, (b) Overview of the stretch sensing using the nanocomposite deposited on the woven elastic fabric.

independent hysteresis behavior, generalized Prandtl-Ishlinskii model was applied to the conductive polymer ink based pressure sensor [42]. This model showed computationally efficient and robust calibration performances.

In this paper, we report the results of our work on a dispenser printing of piezo-resistive nanocomposite that can adhere directly to skin for measuring the joint angle rotation of a user (figure 1). The proposed sensing system can provide comfortable motion sensing without the use of inextensible straps to fix the sensor. Through this approach, the sensing system can be covered (e.g., under clothes) while facilitating long-term and outdoor motion monitoring of patients (figure 1). As the sensing material, a nanocomposite of long multi-walled carbon nanotube (Long-MWCNT) and silicone rubber was developed. Long-MWCNTs have a high aspect ratio that can reduce the weight ratio required to achieve proper conductivity. This weight ratio reduction can lower the viscosity of a liquid state nanocomposite. This low-viscosity liquid-state nanocomposite permeates into a woven elastic fabric to ensure strong adhesion force during the dispenser printing. Contributions of this work are two things. Firstly, cost-effective nanocomposite showing decent sensing performance as well as low viscosity was introduced and dispenser printing of the nanocomposite on the woven elastic fabric was demonstrated. Secondly, the modified Prandtl-Ishlinskii (MPI) model was firstly applied to correct nonlinear hysteresis of the piezo-resistive nanocomposite analytically. As a validation, wrist movement experiments were performed.

2. Manufacturing process of the stretch sensing system

2.1. Long MWCNT/Silicone rubber nanocomposite paste preparation

Piezo-resistive sensing material was fabricated using long-MWCNT as a conductive filler and silicone rubber as a polymer matrix. Mechanical and electrical properties of the composite material vary in relation to the type of conductive filler and to the fabrication method, as well as with the existence of chemical additives [31]. For this reason, suitable materials and fabrication methods had to be selected after careful consideration. In this section, characteristics of the newly developed piezo-resistive material are presented.

To achieve high stretchability, conformable silicone rubber (EcoFlex0030, Smooth-On Inc., USA) was selected as a polymer matrix. The silicone rubber showed an elongation limit of 800%, which is suitable for stretch sensing. In terms of viscosity, however, the silicone rubber showed 3500 cps. Furthermore, it was observed that when the MWCNTs were mixed into the silicone rubber, this viscosity rose to 20 000 cps (nearly 6-times higher than pure silicone rubber). Although widely adopted methods used to disperse nanomaterials into elastomer are solvent casting, freeze drying, spray drying, *in situ* polymerization, melt blending, and solution mixing [43, 44], solution mixing (nano fillers are mixed into the polymer solution by energetic agitation) was utilized due to the high-viscosity matrix.

MWCNT with high aspect ratio (15 000) (CM280, Hanwha Inc., South Korea) was selected as a conductive filler. From the literature [31], it was reported that MWCNTs with high aspect ratio tend to exhibit higher conductivity than those with lower aspect ratio when dispersed into elastomers at the same concentration. This means that nanocomposites made with high aspect ratio of MWCNT should achieve lower viscosity. The viscosity of long-MWCNT/silicone rubber paste is a crucial factor for achieving better dispersion in the solution mixing. In addition, low viscosity of the paste was expected to enhance the adhesive force between the paste and the woven elastic fabric.

The fabrication procedure utilized consisted of two mixing stages (figure 2(a)). In the first stage, MWCNTs and silicone rubber were mixed using a planetary centrifugal mixer (ARE-310, THINKY, USA). This mixer dispersed MWCNT paste uniformly by rotating at 2000 rpm for 10 min. Such revolution causes powerful acceleration that promotes dispersion and, at the same time, the rotation generates convection of the paste inside the container. In the second stage, a shear mixer (80E, EXAKT, Germany) was used to apply more energetic agitation to the paste for 2 min. One example of the mixed liquid state of the long-MWCNT/silicone rubber paste is shown in figure 2(a). To examine the dispersion status of the cured long-MWCNT/silicone rubber paste, scanning electron microscopy (SEM) was conducted. As shown in figure 2(b), the proposed fabrication process enabled homogeneous distribution of MWCNT in the polymer composite.

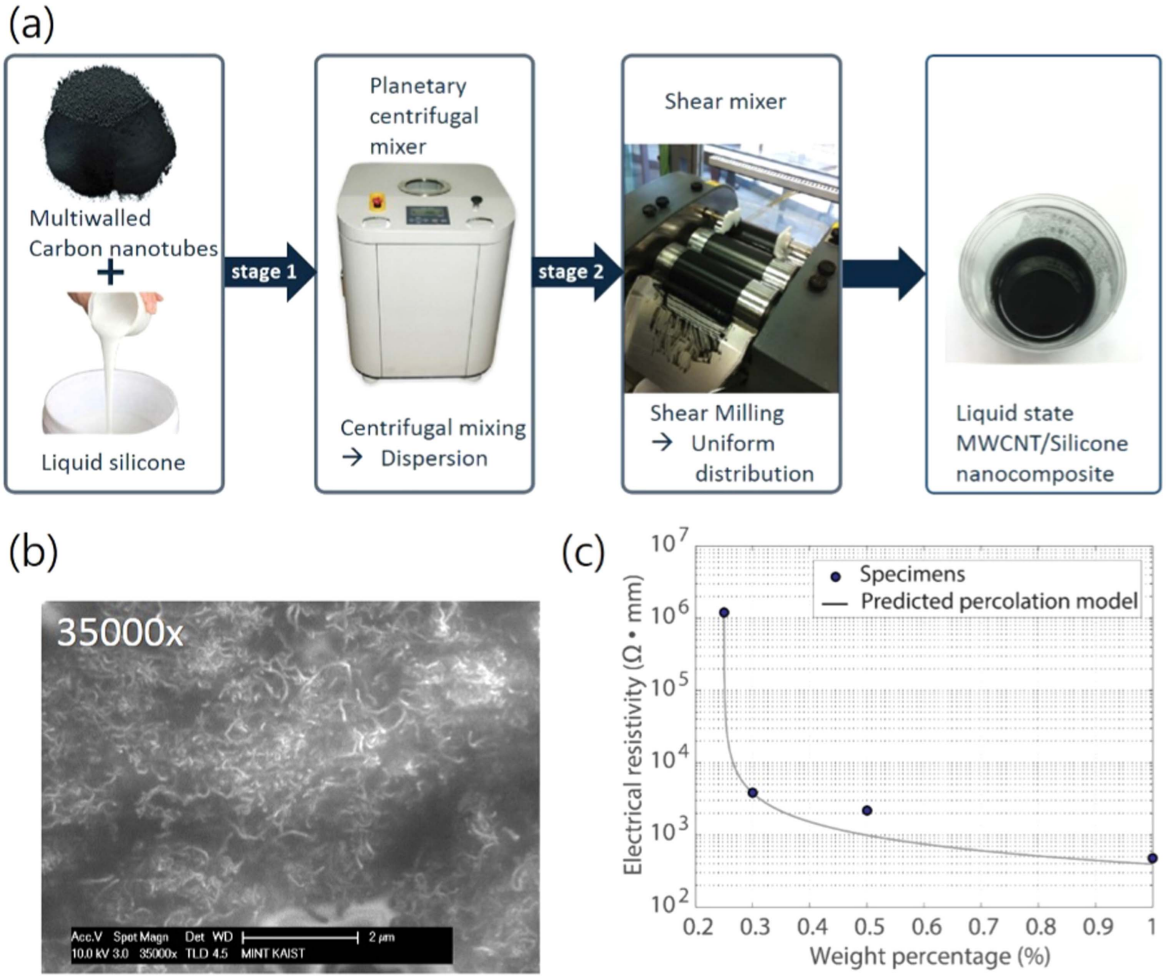

Figure 2. (a) Schematic of the fabrication process, (b) SEM image of homogeneously dispersed MWCNTs captured from the cured nanocomposite, (c) Electrical resistivity in relation to MWCNT concentration in weight percentage.

In order to characterize the electrical resistivity of the paste following the addition of MWCNT, the relationship between the electrical resistivity of the nanocomposite and the MWCNT concentration was examined using four different concentrations (0.25, 0.3, 0.5, and 1 wt%). For each case, the electrical resistivity was measured using a digital multi-meter (15B, Fluke, USA). Figure 2(c) shows that resistivity decreased notably at concentration ratios >0.2 wt%. This is known as the percolation phenomenon, and it explains the formation of conductive pathways through randomly located conductive nanomaterials [45]. The percolation model was predicted from the resistivity of the four cases. It should be noted that long-MWCNT achieves low resistivity at a relatively low concentration ratio. The viscosity of the nanocomposite paste was <5000 cps with 0.5 wt% MWCNT concentration. This viscosity level was low enough to use with the dispenser printing method.

2.2. Dispenser printing of the nanocomposite on the woven elastic fabric

The nanocomposite paste presented in the previous section was used in a dispenser printing method to deposit the paste on a woven elastic fabric. The woven structure of the elastic fabrics can provide permeability for nanocomposite bonding and breathability for long-term usage. To print using liquid nanocomposite paste, an automatic dispenser composed of pneumatic pressure regulator (AD3000C, Iwashita Engineering, Japan) and a 3D manipulator (EzRoBo-5GX, Iwashita Engineering, Japan) was used as shown in figure 3(a). The dispenser provided compressed air to eject the viscous nanocomposite paste through the printing nozzle while tracking a predefined trajectory. Figure 3(b) presents a fabrication schematic for printing of the nanocomposite paste onto the woven elastic fabric (kinesiology tape, TS Co., Ltd., South Korea). The U-shaped specimen is presented in the figure which was used in the preliminary study [46]. This design was utilized for facile wiring for human subject experiment. The fabric showed high stretchability up to 50% strain and it has biocompatible adhesive gel on the other side. Moreover, the adhesive force between the fabric and skin was highly reliable under dynamic motion.

The first step in the fabrication process was positioning the woven fabric on the moving stage of the automatic dispenser. Then, electrodes made of conductive fabric (Shieldex 2611, Startex, USA) were placed on the woven elastic fabric. The conductive fabric has a mesh structure which enables

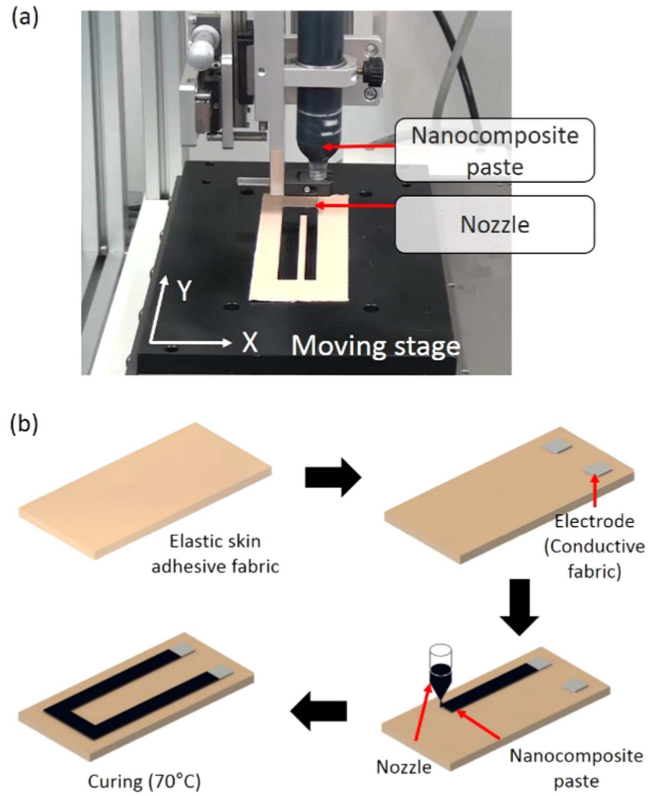

Figure 3. Illustration of (a) Automatic dispenser printing with moving stage and (b) Fabrication procedure of skin-mountable specimen [46].

high stretchability (<20% strain) and high permeability for the nanocomposite paste. The stretchability of the electrode is a necessary feature in wearable motion sensors; otherwise increased contact resistance might occur between the electrode and nanocomposite under dynamic conditions. Moreover, the conductive electrode was adhered to the elastic fabric during the dispenser printing because the paste covered up the mesh-structured conductive electrode and permeated into the fabric. In the next step, the automatic dispenser printed the long-MWCNT/silicone rubber nanocomposite paste onto the woven elastic fabric. During this process, the air pressure driving the paste and the moving speed of the nozzle was controlled to obtain the desired printing thickness. In this work, 40 kPa air pressure and moving speed of 2 mm s^{-1} were used to obtain a printing thickness of 2 mm (See supplementary video 1 is available online at stacks.iop.org/SMS/27/025017/mmedia). The printing speed was limited due to the viscosity of the nanocomposite because the nanocomposite should contact the top surface of the elastic fabric to ensure a consistent printing pattern. This 2 mm thickness was set to obtain low and consistent electrical resistance because the resistivity of the nanocomposite is determined by the conductive percolation network in the nanocomposite. More details about this thickness limitation is described in the discussion section. After the conductive fabric electrode and the woven elastic fabric were covered with nanocomposite paste, the printed composite was cured in an oven (OF-02, Jeiotech, South Korea) for 20 min at 70 °C.

The completed specimen could be stretched to 35% strain as shown in figure 4(a). Because of the highly deformable characteristic of the silicone rubber based nanocomposite, the specimen showed stable attachment between the nanocomposite and the woven elastic fabric (See supplementary video 2). This stable attachment was achieved due to the low viscosity of the nanocomposite paste. Because the nanocomposite paste had low viscosity (near 3500 cps), the paste slightly permeated the micro-gaps in the elastic fabric after printing. Figure 4(b) shows a surface when the nanocomposite and elastic fabric was separated by force. This bonding force was 3.961 N, as measured using a 180 degree T-peel test [37, 47]. This bonding force is strong enough to maintain adhesion between the nanocomposite and the elastic fabric under dynamic conditions. The surface morphology of the permeated region was characterized by field emission scanning electron microscopy (FE-SEM, Sirion, FEI, USA) operating at an acceleration voltage of 10 kV. The specimen was located on carbon tape and a thin (~10 nm) platinum layer was sputtered on for better SEM imaging quality. From the SEM images captured from the permeated region of the nanocomposite, a lattice pattern attributed to threads of the elastic fabric was observed at 100× and 500× magnification (figure 4(c)). This implies that the nanocomposite paste can permeate the elastic fabric surface and achieve strong bonding force by covering the micro-sized nylon fibers.

In terms of fabrication simplicity, this dispenser printing method with this nanocomposite paste enabled simple and cost-effective fabrication for various stretch sensing pattern printing because the stretch sensing patterns are directly printed on the elastic fabric without a pattern mask [18]. By attaching the nanocomposite printed woven elastic fabric directly to the wearer's skin, we achieved a compliant and comfortable motion sensing system without inextensible straps or tight sleeves for long-term usage. Next, to investigate the piezo-resistive characteristics, extension tests were conducted.

3. Characterization of the piezo-resistive nanocomposite

The stretch sensing performance of the piezo-resistive nanocomposite varies considerably in relation to the materials and fabrication processes used, as indicated in the many studies about characteristics of piezo-resistivity [1]. For this reason, the properties of the new long-MWCNT/silicone rubber nanocomposite were determined. Tensile experiments were conducted to assess the piezo-resistivity of the long-MWCNT/silicone rubber nanocomposite. Through these experiments, the effects of the long-MWCNT concentration and variation of specimen dimensions were investigated.

3.1. Experimental setup

The specimen responses to various loading conditions were tested using a custom motorized test bed (figure 5(a)). Using the extensometer, we measured strains, stresses, and electrical

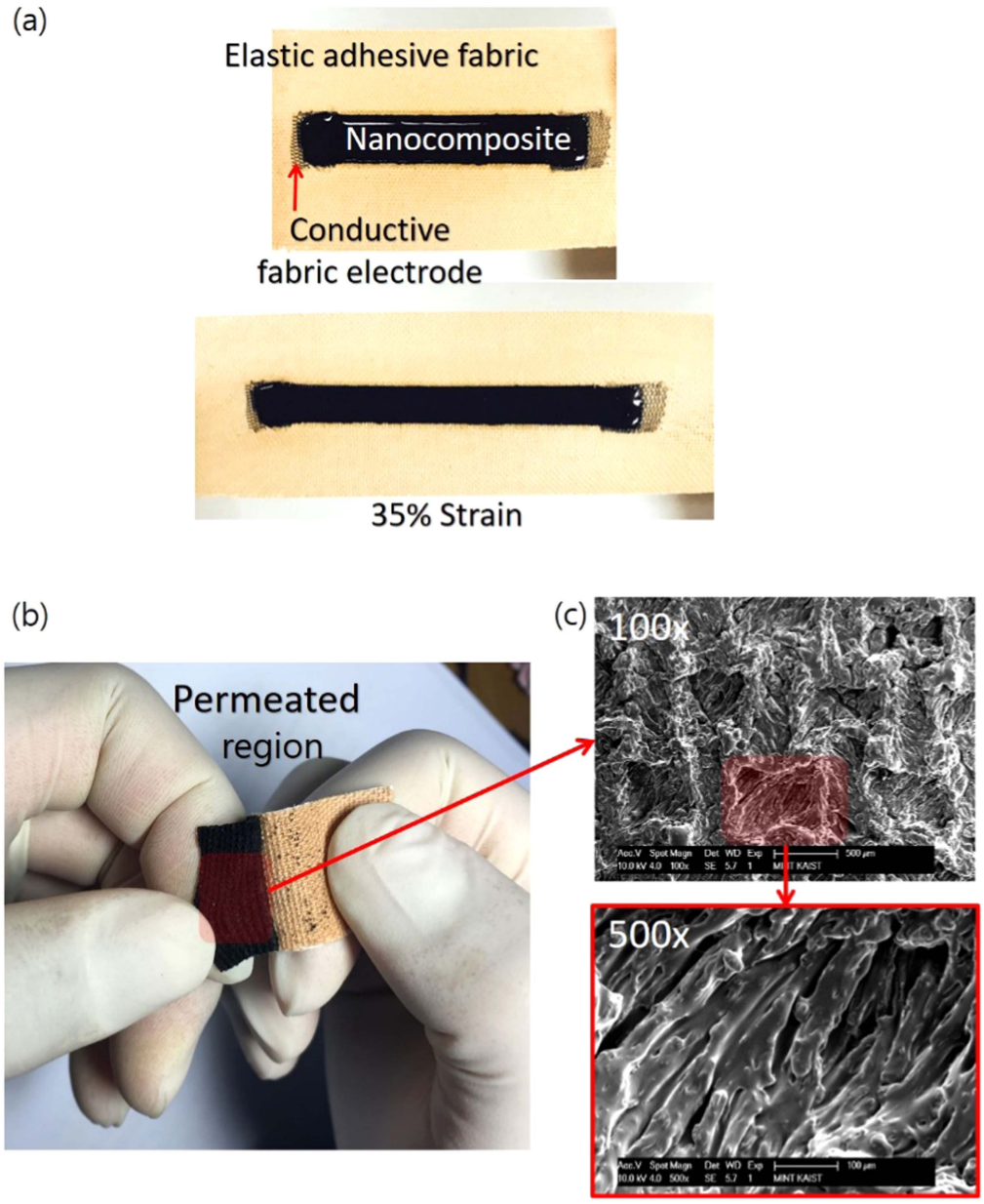

Figure 4. (a) Stretch test to dispenser printed specimen up to 35%, (b) Area showing separation of the printed nanocomposite from the woven elastic fabric, (c) SEM images (magnification at 100× and 500×) of the lattice pattern on the nanocomposite made by the woven structure of the elastic fabric.

resistance of the specimen, simultaneously. Each end of the specimen was fixed mechanically using insulated plastic clamps. Vertical movements of the clamps induced tensile strain in the specimen. The movement trajectories were programmed via Simulink (MATLAB, mathwork, USA) in terms of the stretch profile. A load cell located at the bottom of the clamp measured tensile force during the experiments. Every specimen was made of rectangular film 2 mm thick (figure 5(b)). The width and the length of the specimens were modulated to examine the effect of dimensional change. Changes in resistivity were calculated using a constant voltage Wheatstone bridge circuit [48], as shown in figure 5(c). From these experiments, the sensitivity, linearity, and hysteresis of the specimens were analyzed because these characteristics are the most important factors in evaluation of the performance of the stretch sensors.

3.2. Effect of the Long-MWCNT concentration

While piezo-resistivity of the nanocomposite results from the formation and destruction of conductive pathways, the amount of conductive nanomaterial in a certain volume strongly affects the formation of conductive pathways [45]. Several types of research have determined that the sensitivity of the nanocomposite can be modulated by controlling the amount of conductive nanomaterial because less nanocomposite results in fewer conductive pathways [49, 50]. Nanocomposites with fewer conductive pathways have higher

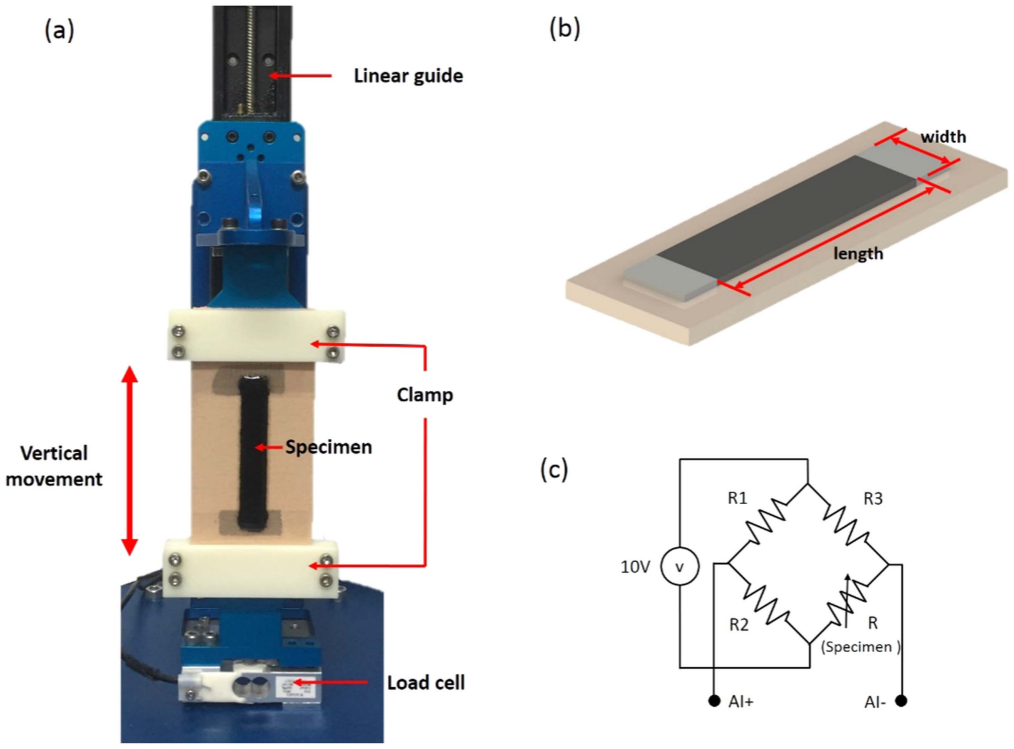

Figure 5. (a) Illustration of custom extensometer consisting of force sensor, linear guided actuator, (b) Schematic of the specimen, (c) Wheatstone bridge circuit of the specimen and hardware configuration.

sensitivity because stretching of the nanocomposite results in the interruption of the conductive pathways.

To examine the influence of long-MWCNT concentration on the sensitivity, five specimens for each of the three different weight ratios of the long-MWCNT and the silicone rubber (0.2, 0.3, and 0.5 wt%) were prepared. Specimens with weight ratios <0.2 wt% and >0.5 wt% were excluded from this study, due to their overly high resistivity or high viscosity. The initial resistance of the specimens was (712.4 ± 310.6, 49.2 ± 17.8, and 7.2 ± 1.4) kΩ for the (0.2, 0.3, and 0.5) wt% specimens, respectively. This great reduction of the initial resistance corresponds to the percolation phenomenon shown in figure 2(c). Following percolation theory [45], the number of conductive pathways increases abruptly and saturates the medium when the concentration exceeds a certain weight ratio. The dimensions of the specimens were the same (40 mm long, 8 mm wide). To simplify analysis, a sinusoidal tensile strain with amplitude of 40% strain at 0.25 Hz was applied during the experiment.

The experimental results presented in figure 6 show the mean and the standard deviation of sensitivity of the three different weight ratio cases following the tensile strain. The sensitivity of the specimens was defined as $(\Delta R/R0)/\varepsilon$ in percentages. The resistance of the specimens increased exponentially with extension in the range of 0%–40% strain. The piezo-resistive linearity of the specimens was approximately identical despite change of the long-MWCNT concentration. From 0 to 40% strain, the sensitivities were 7.87, 2.25, and 1.75 for (0.2, 0.3, 0.5) wt% of long-MWCNT within the polymer matrix. To achieve relatively high

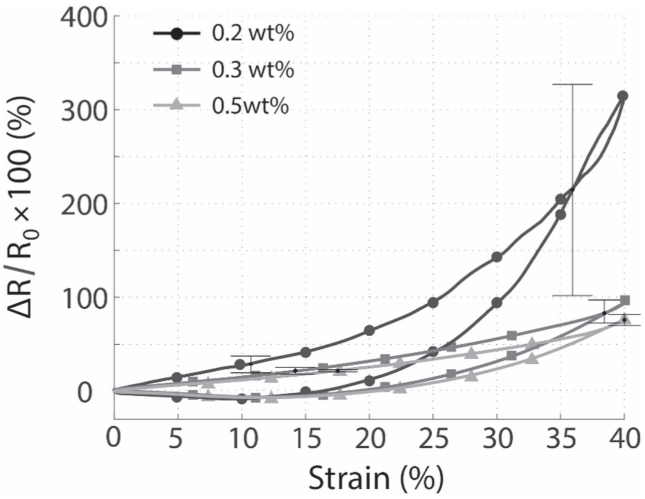

Figure 6. Experimental results of mean and standard deviation of the tensile strain versus sensitivity.

sensitivity, a weight percent of 0.2 wt% would be preferable. However, remarkably large variation of sensitivity was observed even in the case of 0.2 wt%. In general, consistent characteristics were difficult to achieve with low weight percentage due to fortuitous nature of the percolation phenomenon [31]. For a printable stretch sensor, consistency is critical for prediction of the performance of a sensor when the sensor is printed in various shapes. Although the viscosity of the nanocomposite paste slightly increases with increasing concentration ratio, the consistency of the piezo-resistive characteristics was noticeably improved. Therefore, the

long-MWCNT weight percent of 0.5 wt% was selected for use in this work.

3.3. Effects of change in specimen dimensions

To examine the effects of change in dimension on stretch sensing performance, experiments were performed on specimens of different sizes. The lengths and the widths of the specimens were modulated. As shown in figure 5(b), the two electrodes are connected through the nanocomposite. The resistivity of the nanocomposite is determined by the number of the conductive pathways formed between the electrodes on the edges. The random dispersion of the long-MWCNTs in the nanocomposite, compel these conductive pathways to be generated in random directions. This implies that an increase in the distance between electrodes could reduce the potential for having conductive pathways. Meanwhile, an increase of the width between the electrodes could result in the opposite effect. Via these experiments, we investigated dimensional effect on the piezo-resistivity.

Two types of experiments were prepared. The first type involved modulating the specimen length while the specimen width was kept constant. For this experiment, specimens with three lengths (20, 40, and 60) mm and width of 8 mm were prepared. The second experiment involved modulating the specimen width (4, 8, and 12) mm, while the specimen length was maintained at 40 mm. As in the previous section, a sinusoidal tensile strain with amplitude of 40% strain at 0.25 Hz was applied.

The results are presented in figure 7. From the change in length, the initial resistance of the specimens was (3.32, 8.98, and 10.30) kΩ for (20, 40, and 60) mm length, respectively. The sensitivity increased to 0.85, 2.92, and 6.67 in relation to increased length (figure 7(a)). In the case of change in the width, the initial resistance of the specimens was (8.98, 6.35, and 7.53) kΩ for (4, 8, and 12) mm width. The sensitivities of these specimens decreased to 2.92, 1.56, and 1.05, respectively. These results imply that sensing performance can be manipulated by adjusting the printing shape, even if using the same nanocomposite. To increase the stretch sensing sensitivity, a narrow (proportionally longer) shape could be adopted, while a wider shape could be used to achieve less nonlinearity.

3.4. Effect of the stretch speeds

The effect of the stretch speeds was also examined to evaluate the dynamic characteristic of the nanocomposite resistivity. Sinusoidal extension with 40% strain at three different frequencies (0.25, 0.5, and 1 Hz) was applied to a specimen 40 mm long and 8 mm wide. The frequency range was selected considering human joint motion.

Figure 8 shows the results of the experiment. The sensitivity of the specimen increased in relation to the stretch speed (figure 8(a)). From figure 8(a), it can be seen that changes in the stretch speed caused an 18% increase in sensitivity. The viscoelastic behavior is clearly observed in the stress versus strain curve in figure 8(b). An increase of the

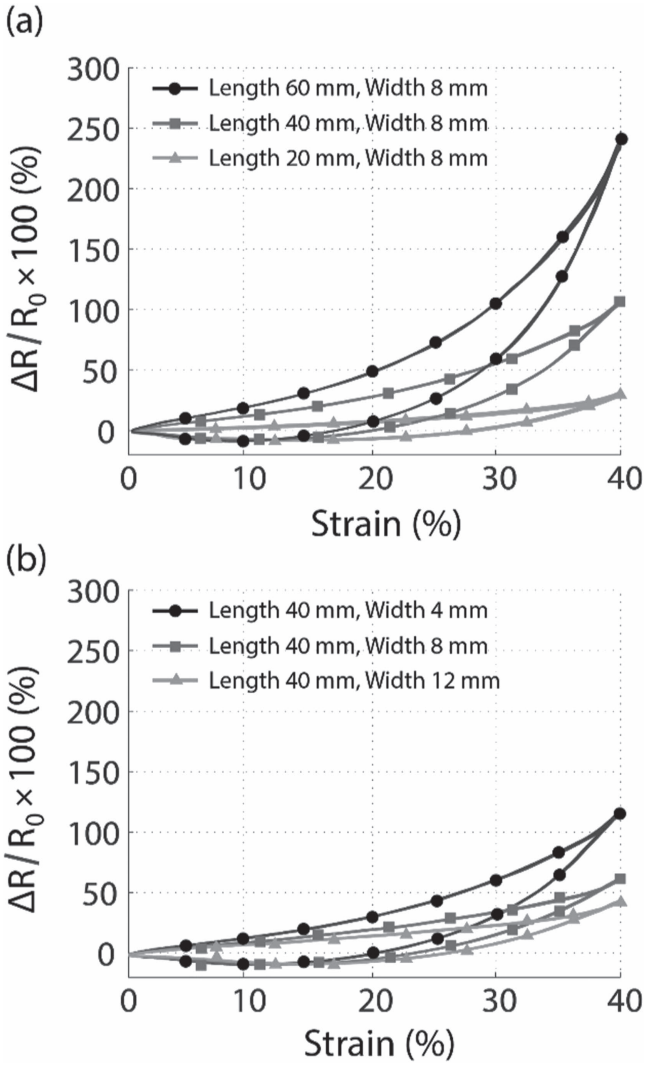

Figure 7. Experimental results of normalized resistance change versus strain for (a) Specimens of three different lengths (same width), and (b) Specimens of three different widths (same length).

stretch speed resulted in an increase in energy dissipation of the viscous nanocomposite. This viscoelasticity of the nanocomposite seems to cause the sensitivity increase when the nanocomposite is stretched. In viscoelastic materials, the effect of damping becomes dominant if strain is applied rapidly. This means that fast stretching can exert more stress in a local region of the nanocomposite. This could break conductive pathways and finally result in greater change in resistivity. However, the hysteresis behavior remained, even when the nanocomposite was stretched very slowly, which can be considered a quasi-static condition. This means that the hysteresis behavior not only is caused by the viscoelasticity of the silicone rubber, but also by rate-independent factors such as residual strains or static friction between MWCNTs [39].

3.5. Temperature reliability

In general, the resistivity of nanocomposites is susceptible to temperature change because heat energy excites the electrons

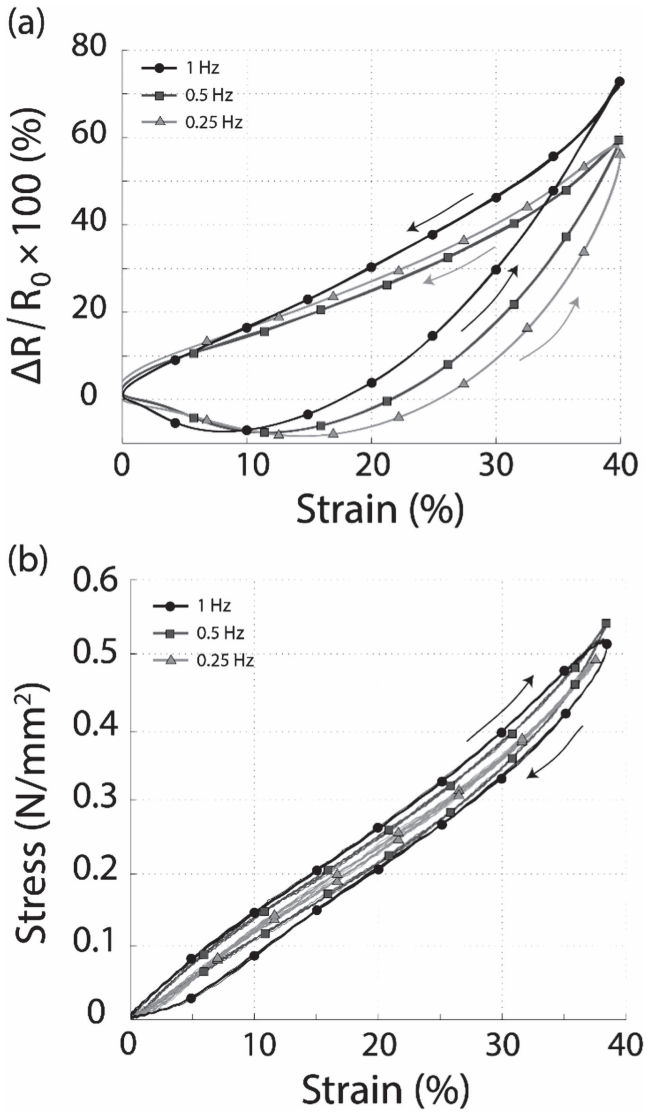

Figure 8. Experimental results of normalized resistance change versus strain for three different stretch speeds.

in the nanocomposite, allowing some electrons to penetrate the insulating polymer [51]. This tunneling conductivity phenomenon is generally known to result in a decrease in resistivity. For these tests, a range of temperatures (30–70 °C at 5 °C intervals) was used. The temperature was controlled by an oven (OF-02, Jeiotech, South Korea). The heat was maintained for 10 min to provide sufficient heat transfer at each temperature interval. As shown in figure 9(a), the resistance of the specimen decreases with increase in temperature.

Regarding hysteresis behavior, mechanical stiffness decreases and viscosity increases with increasing temperature for silicone rubber [52, 53]. Definitely, this can also affect hysteresis behavior of the piezo-resistivity [54]. To investigate this effect, the ambient temperature was heated up from 25 Celsius degree to 55.5 Celsius degree using a standing heater. The temperature was maintained during the cyclic extension test. The test was conducted to a 40 mm length and 8 mm width specimen under 30% extension strain and 0.25 Hz of frequency. As a result, nearly 60% sensitivity change and noticeable hysteresis change was observed (figure 9(b)). This result can be caused by the mechanical property change and tunneling conductivity change following to the temperature elevation.

The major application of the proposed nanocomposite is skin-mountable motion sensing, which means that the nanocomposite (once installed) would be expected to experience a constant temperature. For this reason, temperature effect was neglected in this study. However, considering broad applications of the printing nanocomposite, this temperature effect needs to be studied further in the future to address the phenomenon and compensate the effect.

4. Hysteresis correction for stretch estimation

4.1. Modified Prandtl-Ishlinskii (MPI) model

Nanocomposites are known to possess noticeable amounts of nonlinear piezo-resistive hysteresis due to many factors, including such as friction force between nanomaterials, viscoelasticity of the nanocomposite, and irreversible changes in polymer fibers [39]. Although mechanically stiff, nanocomposites generally tend to exhibit low hysteresis, meaning that soft and stretchable nanocomposites are required to implement skin-adhesive stretch sensors. For this reason, a nonlinear hysteresis correction is necessary to improve the angle estimation accuracy of the stretch sensor.

As shown in the previous chapter, the effects of hysteresis and nonlinear behavior were observed from the long-MWCNT/silicone rubber nanocomposite. First, the nanocomposite exhibited exponentially increasing sensitivity in relation to the amount of stretch. Furthermore, negative sensitivity was observed in the region near the initial stretch. Second, the resistance change curve followed a different path after the nanocomposite recovered from a stretch. This curve clearly draws a counter-clockwise loop from the stretch to the recovery. Due to this behavior, considerable stretch estimation error was produced using this stretch sensor.

To correct for hysteresis, a mathematical formulation of the hysteresis is required, and much research has been done using mathematical hysteresis models including such as the Preisach model, the Prandtl-Ishilinskii (PI) model, and the Duhem model [55]. Among these, the Modified Prandtl-Ishilinskii (MPI) model is applied for skin-mountable stretch sensing [56]. The MPI model formulates rate-independent and monotonic hysteresis behavior. This means this model can compensate velocity independent and monotonic piezo-resistive characteristics of the nanocomposite. Although the nanocomposite possesses certain amount of rate-dependent and non-monotonic behavior, the overall behavior matched with MPI model. More importantly, the MPI model makes it easier to calculate inverse of hysteresis analytically. This easy calculation is beneficial for implementing real-time applications where rapid inverse calculations are essential.

The MPI model adopted in this paper consists of two elementary hysteresis operators [56]. One is the play operator,

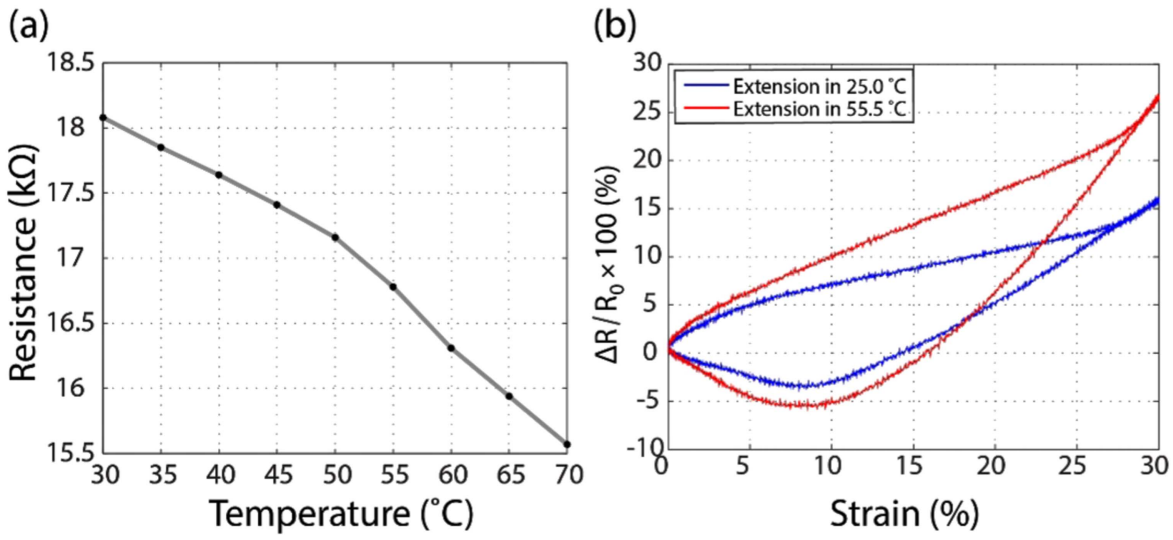

Figure 9. Experimental results of (a) the initial resistance change versus temperature and (b) the resistance change versus extension strain at the room temperature and the elevated temperature.

which is rate-independent. The play operator $H_{rh}[x](t)$ with threshold $r_h \geqslant 0$ for any piecewise monotone input function $x(t)$ is defined as

$$y(t) = H_{r_h}[x, y_0](t)$$
$$H_{r_h}[x, y_0] = \max\{x(t) - r, \min(x(t) + r, y(t - T)\} \quad (1)$$

where y_0 is the initial value of the output function and T is the sampling period. The sampling period T is used to define the previous output value.

The play operator was utilized to obtain enhanced hysteretic nonlinearity through linear weighted superposition. Multiplying the operator (with threshold of r_h) by a weight value w_h, the linear weighted play operator is defined as

$$y(t) = \mathbf{w}_h \cdot \mathbf{H}_{\mathbf{r}_h}[x, \mathbf{y}_0](t) \quad (2)$$

where the weight vector $\boldsymbol{w_h}^{\mathrm{T}} = [w_{h0} \ \ldots \ w_{hn}]$ and $\boldsymbol{H_r}[x, \boldsymbol{y_0}](t) = [H_{r0}[x, y_{00}](t) \ \ldots \ H_{rn}[x, y_{0n}](t)]^{\mathrm{T}}$ with the threshold vector $\boldsymbol{r_h} = [r_0 \ \ldots \ r_n]^{\mathrm{T}}$ where $0 = r_0 < \ldots < r_n$, and the initial state vector $\boldsymbol{y_0} = [y_{00} \ \ldots \ y_{0n}]^{\mathrm{T}}$. The order of the play operator (n) determines the smoothness of the approximation. To estimate nonlinear hysteresis behavior, the order of the play operator adopted must be sufficiently high.

The other operator is the one-sided dead-zone operator, which models complex hysteretic nonlinearity. This dead-zone operator is defined as

$$y(t) = S_{r_s}[x](t)$$
$$S_{r_s}(x(t), r_s) = \begin{cases} \max\{x(t) - r_s, 0\} & r_s > 0 \\ x(t) & r_s = 0 \end{cases} \quad (3)$$

In this operator, threshold r_s determines the output. Similar to the play operator, the dead-zone operator is also multiplied with the constants to obtain linear weighted superposition.

$$y(t) = \mathbf{w}_s \cdot \mathbf{S}_{\mathbf{r}_s}[x](t) \quad (4)$$

where the weight vector $\boldsymbol{w_s}^{\mathrm{T}} = [w_{s0} \ \ldots \ w_{sn}]$ and $\boldsymbol{S_r}[x](t) = [S_{r0}[x, y_{00}](t) \ \ldots \ S_{rn}[x, y_{0n}](t)]^{\mathrm{T}}$ with the threshold vector $\boldsymbol{r_s} = [r_0 \ \ldots \ r_n]^{\mathrm{T}}$ where $0 = r_0 < \ldots < r_n$.

The complete form of the MPI operator is obtained by combining the weighted play operators and the weighted dead-zone operators as follows.

$$\Gamma[x](t) := \mathbf{w}_s^T \cdot \mathbf{S}_{\mathbf{r}_s}[\mathbf{w}_h \cdot \mathbf{H}_{\mathbf{r}_h}[x, \mathbf{y}_0]](t) \quad (5)$$

From this strategy, nonlinear and asymmetric hysteretic behavior was easily formulated analytically using linear combination of the operators. These operators were also simply determined using previous output values or thresholds. As mentioned before as an advantage of MPI model, this facile formulation enabled fast and accurate inverse calculation and identification of parameters in practical applications.

For the case of inverse calculation, the inverse MPI model was obtained by exchanging the calculation order and transforming the parameters, including the weighting constants ($\boldsymbol{w_h}$, $\boldsymbol{w_s}$), thresholds ($\boldsymbol{r_h}$, $\boldsymbol{r_s}$), and initial state values ($\boldsymbol{y_0}$).

$$\Gamma^{-1}[y](t) := \mathbf{w}'h^T \cdot \mathbf{H}_{\mathbf{r}'h}[\mathbf{w}'s^T \cdot \mathbf{S}_{\mathbf{r}'s}[\mathbf{y}'_0]](t) \quad (6)$$

As shown above, equation (6) describes the inverse MPI operator. An interesting feature of this model is that both play and dead-zone operators remain the same even with inverse calculation. The parameters with the prime symbol ($\mathbf{w}'_{\mathrm{h}}$, $\mathbf{w}'_{\mathrm{s}}$, $\mathbf{r}'_{\mathrm{h}}$, $\mathbf{r}'_{\mathrm{s}}$, $\mathbf{y}'_0$) represent the transformed weighting constants, thresholds, and initial output values, respectively. The transformed parameters are analytically determined due to the inherent monotonicity of the play and dead-zone operators. The detailed information needed to obtain these transformed values is provided in the appendix.

In order to implement real-time hysteresis correction for the stretch sensing, the transformed parameters are required to estimate the amount of stretch using the change in resistance. Compared to other hysteresis models, it is relatively easy to identify the parameters of the MPI model because the

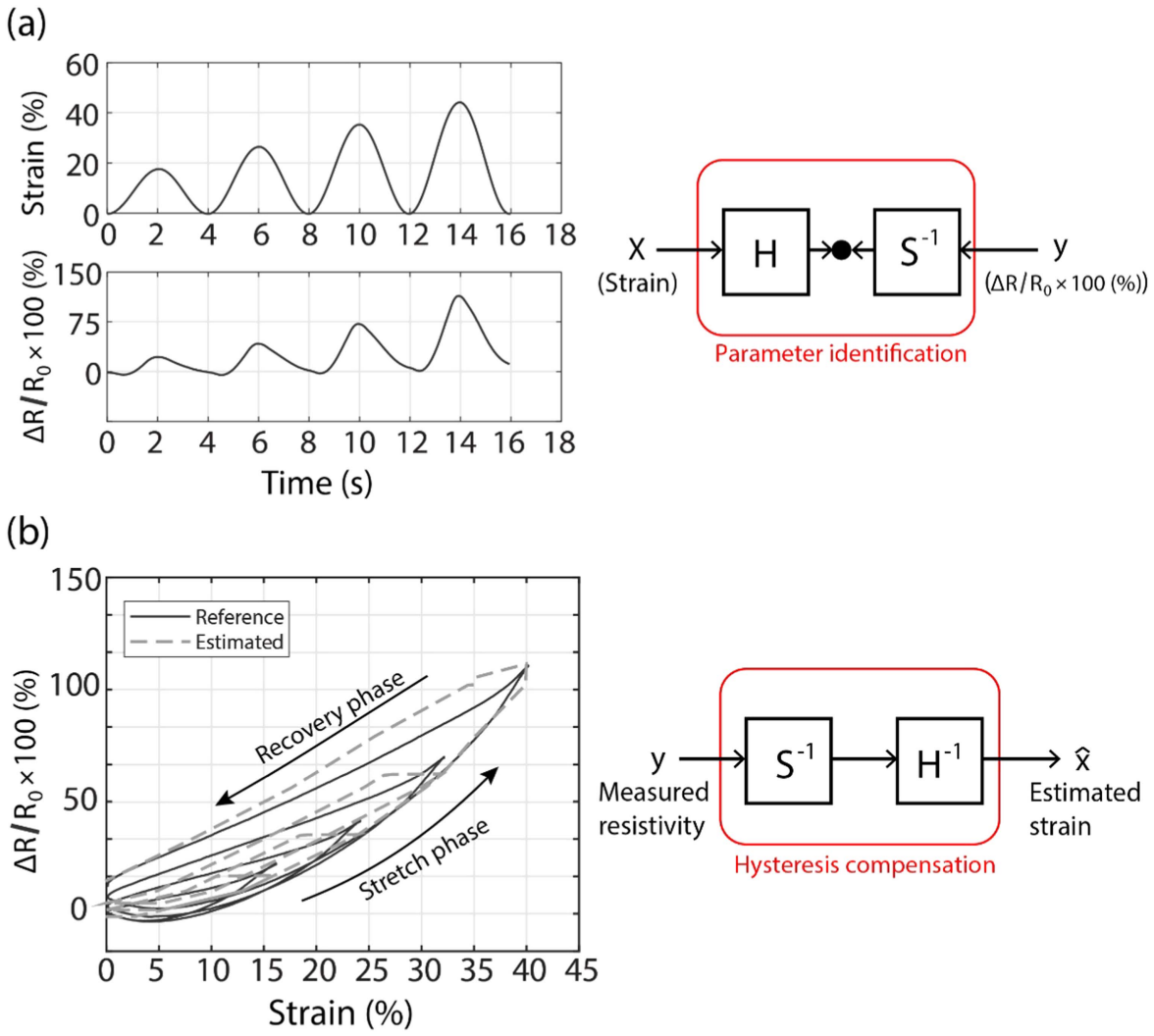

Figure 10. Experimental results showing (a) Stretch experiment and schematic of the parameter identification process (b) Estimated curve from MPI model with reference and schematic of the hysteresis compensation.

invertibility of the MPI model is guaranteed analytically. Moreover, identification is possible with fewer input and output signals.

The identification leads to the quadratic optimization problem that formulates the input with the weighted play operator, and outputs data using the inverse dead-zone operator to minimize the generalized error, as presented below.

$$f_e(x(t), y(t)) := \mathbf{w}_h \cdot \mathbf{H}_{\mathbf{r}_h}[x(t), \mathbf{y}_0] - \mathbf{w}' s^T \cdot \mathbf{S}_{\mathbf{r}'s}[\mathbf{y}(t)] \quad (7)$$

The details of this process were introduced and discussed in the literature [56]. The equations of the MPI model can be applied without modification in this study.

4.2. Stretch estimation experiments

To evaluate the performance of this hysteresis correction, a specimen 40 mm long and 8 mm wide was tested using the extensometer. The specimen was stretched following a sinusoidal trajectory to apply various amounts (20%–40%) of strain at 0.25 Hz. The amplitudes were changed to identify the parameters of the MPI model by changing the extremity value. Figure 10(a) shows the input strain with the resulting resistance change curve. As introduced before, the nanocomposite of the specimen revealed asymmetric nonlinear hysteresis behavior. When the strain phase was changed from stretch to recovery, this turning point is important because the extremity value determines the resistance recovery path of the stretch sensor. In general, gathering input and output data that includes many turning points is favorable for modeling hysteresis behavior, but the MPI model requires fewer turning points to identify the model parameters.

From the identification process, the orders of the play operator and dead-zone operator should be determined in advance. Although higher-order operators can improve the identification accuracy, calculation time also increases. For this reason, the orders selected for this experiment were 50 and 10, respectively. This means that 50 play operators and 10 dead-zone operators that had different weighting constants and thresholds were used to constitute the equation (7). As

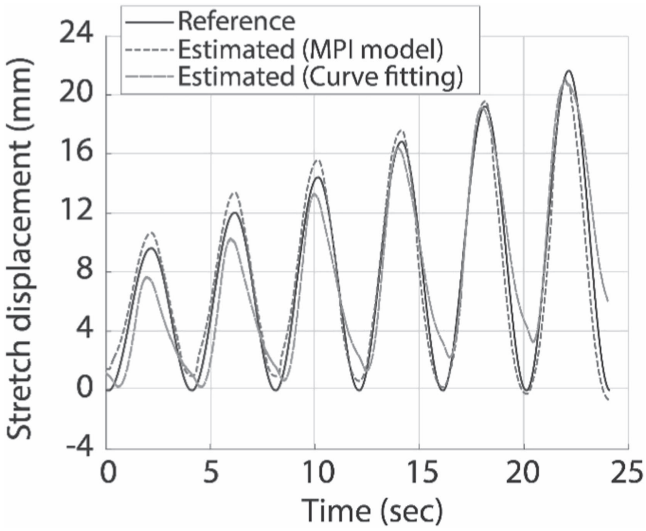

Figure 11. Results of estimated stretch displacement from inverse MPI and third-order polynomial models.

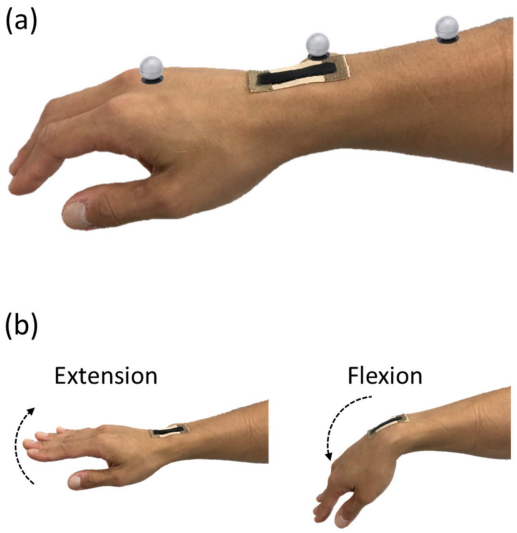

Figure 12. Illustrations showing (a) Experimental setup for wrist flexion and (b) Demonstrations of wrist extension and flexion motions.

illustrated in figure 10(a), the parameters of the play operators ($\mathbf{H}$) and the inverse dead-zone operators ($\mathbf{S}^{-1}$) were obtained by minimizing the equation (7). Using these parameters (including weight constants, thresholds, and initial state values), identified MPI model is presented in figure 10(b). From the results, the modeling error was 3.44 ± 2.17%. The maximum estimation errors occurred at the turning points (shift to recovery from stretch phase and to stretch from recovery phase). From the recovery to stretch phase, the modeling error was caused by non-monotonic resistance with change from 0 to 5% strain. From the stretch to recovery phase, maximum error of 10% was observed due to great change in the asymmetric resistance. Although this error is not negligible, the hysteresis model provides better performance than a high-order polynomial curve fitting model, which showed an modeling error of 5.84 ± 5.18%. Using the hysteresis model, measured resistivity of the nanocomposite can be converted to hysteresis compensated strain as illustrated in figure 10(b).

For validation, the experiment was conducted using the extensometer. The specimen was stretched from 10 to 22 mm (25 to 55% strain) in 0.25 Hz. Figure 11 shows the results of the stretch estimation using inverse MPI model and third-order polynomial curve fitting model. The estimation results clearly show enhanced performance relative to a third-order polynomial model, for the stretch to recovery phase. This phase possesses high hysteresis because the specimen is restored to its original length in response to the elastic restoring force of the nanocomposite. According to the experimental results, the estimation error was 1.05 ± 0.79 mm (5.0 ± 3.9% for 20 mm stretch) using the inverse MPI model and 1.61 ± 1.17 mm (8.1 ± 5.9% for 20 mm stretch) using the third-order polynomial model. The estimation error was reduced to 3.1% when MPI model was applied instead of the third-order polynomial model.

5. Human motion monitoring: wrist angle rotation

For validation, the new stretch sensing sensor was applied to a human subject to estimate wrist angle rotation. The purpose of this study was to evaluate the performance of the nanocomposite printed woven elastic fabric when it is attached to human skin. Because the sensor attached to the skin changes its length proportionally following wrist angle rotation, the change in resistance measured by the sensor can be used to estimate the rotation angle. In this process, hysteresis behavior of resistance change was compensated by the MPI hysteresis model and by the polynomial curve fitting model for comparison.

5.1. Experimental setup

A motion capture system that consisted of 10 infrared cameras was used (Hawk and Ospray, Motion analysis, USA) to measure the reference joint angles. As shown in figure 12(a), a total of three markers were attached to the edge of proximal phalanges, carpal bone of the hand, and upper forearm. The sampling frequency of the kinematic data was 200 Hz and the data were filtered using a Butterworth fifth-order low-pass filter with a cut-off frequency of 10 Hz to eliminate high-frequency noise and to avoid significant filtering distortion in the data.

One healthy subject (30 years old) with no history of musculoskeletal disease in his upper extremities participated in this experiment. The subject signed informed consent forms approved by the KAIST Internal Review Board (IRB) Committee prior to the experiments. In this test, wrist joint angles in the sagittal plane were measured during flexion and extension motions of the wrist, as shown in figure 12(b). The stretch sensor was attached to the skin in the extension condition because the sensor can only measure elongation. The change in the resistance of the stretch sensor was measured using the bridge circuit shown in figure 5(c); then converted

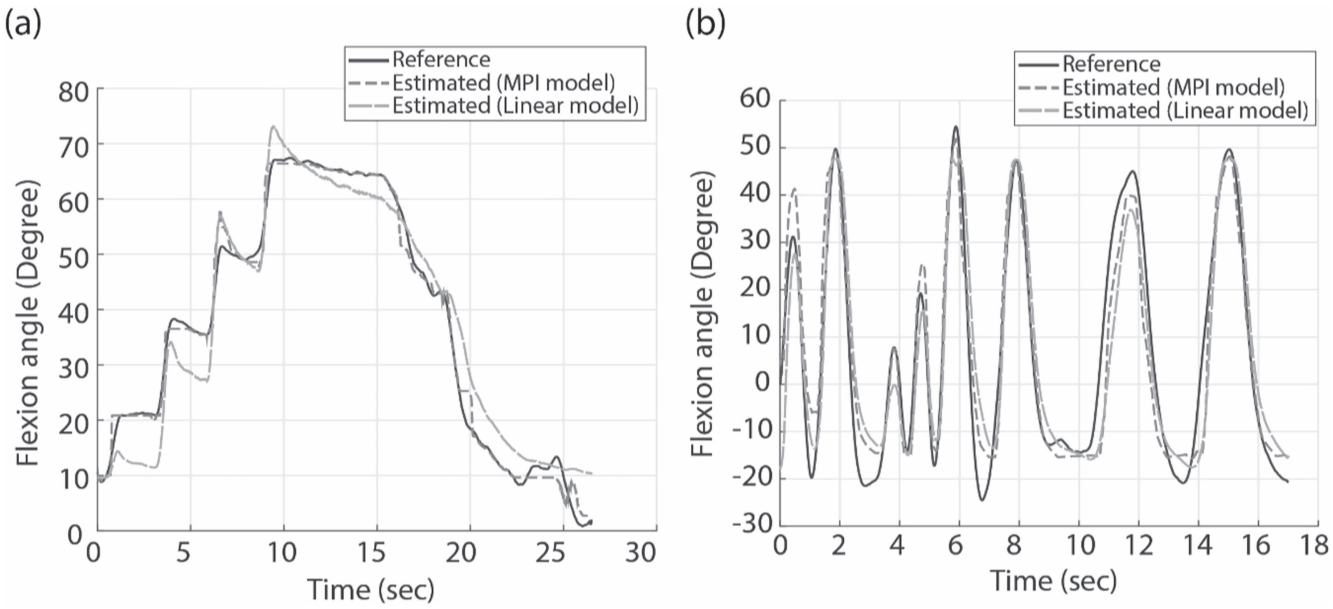

Figure 13. Experimental results of the flexion angle estimation for (a) Step increment and decrement wrist movements and (b) Arbitrary wrist movements.

to the flexion angle using the inverse MPI model. The parameters of the inverse MPI model were estimated using reference data obtained from the motion capture system. These parameters were used to calculate the flexion angle in real-time. The orders of the operators chosen were 50 and 10 for play operators and dead-zone operators, respectively. For the validation test, two wrist motions were conducted. The first motion was step increment flexion movement. The second motion was arbitrary flexion movement.

5.2. Results

Figure 13 shows the experimental results of the two wrist motions. The flexion angle was estimated using the inverse MPI and third-order polynomial models. From the step increasing and decreasing movements, the wrist was rotated and stopped for more than two seconds, as shown in figure 13(a). The estimation errors were 1.93 degrees for the MPI model and 5.43 degrees for the third-order polynomial model. While the movement was fixed, change in the resistance occurred due to mechanical relaxation of the stretch sensor. This characteristic produced an estimation error in both cases. However, a large estimation error occurred in the step decrement movements. As explained before in section 4.2, this is caused by a difference between the stretch and recovery mechanisms. This result signifies the necessity of the hysteresis correction for the stretch sensor.

For arbitrary wrist flexion movements, the experimental results are presented in figure 13(b). The flexion angle was modulated between -20 degrees and 55 degrees at various movement speeds. The estimation errors were 7.15 degrees for the MPI model and 8.75 for the third-order polynomial model. The estimation errors increased for arbitrary wrist movements. The main reason for this increase in the error is assumed to be residual strain. From high speed movements, recovery time was insufficient for the stretch sensor when the sensor was in the recovery to stretch phase. Due to this situation, a certain amount of the strain remained inside of the stretch sensor and this residual strain prevented the sensor from recovering to its original length during the recovery to stretch phase. These large errors were observed in the experimental results when the flexion angle was <-10 degrees. Despite this limitation, the estimation error was relatively low when hysteresis behavior was corrected.

6. Discussion and conclusions

In this study, dispenser printing of long-MWNCT/silicone rubber nanocomposite on the woven elastic fabric is introduced to manufacture a new skin-mountable stretch sensor that can be attached directly to human skin. The woven elastic fabric was utilized as an intermediate layer between the nanocomposite and the skin to prevent direct contact of the nanocomposite with the skin. Considering the manufactural advantage of the dispenser printing, the stretch sensor can provide cost-effective wearable motion sensing feature. Moreover, in terms of wearability, this stretch sensor is a great improvement because it can be attached to the skin without any strips or sleeves. This advantage enables less rigid and more comfortable motion sensing compared to previous sensing systems.

To achieve this objective, two issues were faced in this study. The first issue was achieving sufficient bonding force between the nanocomposite and the elastic substrate because low bonding force causes exfoliation of the nanocomposite from the substrate. To enhance the bonding force, a piezoresistive nanocomposite paste with low viscosity was developed using long-MWCNT. Due to its low viscosity (near 3500 cps), the nanocomposite paste could permeate micro

gaps in the elastic fabric and achieve a strong bond. This result was verified using SEM imaging and a 180 degree T-peel test. The method proposed for printing with nanocomposite paste, made it easy to adjust the dimensions of the sensors with stretchability up to 35% strains. To improve manufacturability of the stretch sensor in the future, the printing speed needs to be improved as much as the printing speed of the ink-jet printing through modifying rheological characteristic of the silicone rubber.

Beside the mechanical characteristics of the long-MWCNT/silicone rubber nanocomposite, the electrical characteristics of the nanocomposite was also investigated in this study. From the experimental results, the effects of the long-MWCNT concentration, dimensional change, and stretch speeds were examined. The characteristics of the nanocomposite were explained qualitatively by the percolation theory [45]. This means that characteristics of the printed nanocomposite can be optimized through this theory to obtain proper stretch sensing performance. As a printable stretch sensor, consistent resistivity is crucial as well as high sensitivity because the nanocomposite can be designed and printed in various patterns. To obtain consistent resistivity, high long-MWNCT concentration along with wide and thick printing pattern was preferable. In this study, 0.5 wt% long-MWCNT concentration and 2 mm printing thickness was set for this reason. This is a limitation of the long-MWCNT/Silicone rubber nanocomposite. To print thin and slender printing patterns, new conductive particles [49] or dispersion methods [57] which form a dense conductive network can be a promising approach in the future. As the piezo-resistive characteristics can be determined by the width and the length of the nanocomposite between two electrodes, the characteristics of the U-shaped specimen as shown in figure 3 can be regarded as a single strip specimen which has the same length.

The second issue was correcting for nonlinear and high hysteresis behavior of the piezo-resistive nanocomposite. From the tensile test at various stretch frequencies, hysteresis behaviors with both rate-dependent and rate-independent features were observed. In this study, the modified Prandtl-Ishilinskii (MPI) model was adopted to correct rate-independent hysteresis behavior of the resistance change measured from the stretch sensor.

From the tensile test, the stretch displacement was estimated using normalized resistivity change and MPI model. Although the parameters of the MPI model was obtained from 0.25 Hz stretch experiment, the MPI model could improve the stretch strain estimation performance compared to the curve fitting model by correcting the hysteresis effect that mostly results during the recovery from flexion phase.

For validation of the sensing capability of the sensor, wrist movement tests were conducted. In the tests, the nanocomposite printed elastic fabric was attached to the fully extended wrist because the stretch sensor can only measure elongation. Although slight compression strain can be applied to the sensor during the wrist movement due to motion artifact or movement of the skin, the 10% compressive strain showed nearly 3% resistivity change. Regarding the fact that the resistivity change of extension mode under 10% strain also shows low sensitivity, the effect of compression is not negligible. To reduce this compression effect, the sensor needs to be pre-stretched when attached to the wrist. The wrist flexion angle in the sagittal plane was estimated with real-time hysteresis correction. The estimation errors were 1.93 degrees (2.9%) for the step increment and decrement test and 7.15 degrees (9.5%) for the arbitrary movement test. Although this amount of error is not negligible compared to stretch sensors made of liquid metal or conductive liquid [6, 58], still hysteresis correction improved the stretch estimation performance of the stretch sensor fabricated using nanocomposite printing. Regarding to the stretch speed dependent sensitivity change, this estimation error can be improved by adopting rate-dependent hysteresis compensation model such as Duhem model [55] in the future. Nevertheless, MPI model provided moderate hysteresis compensation performance even with small calibration dataset. This feature can be beneficial for user-specific designed stretch sensors.

In the future, the proposed sensor could offer improved motion sensing systems if several limitations are resolved. The remaining drawbacks of the proposed sensor are non-monotonic piezo-resistivity and residual strains. These factors cause increase of the estimation error in the hysteresis correction. Despite of these errors, the proposed stretch sensor showed a potential for estimating the rotation angles of human joints while providing comfortable motion sensing. Another drawback is that the sensor can only measure the amount of stretch. Due to this limitation, the stretch sensor was mounted to the wrist joint when it is totally extended. For future research, this limitation can be resolved using multiple stretch sensors attached on the opposite side of the wrist. In this study, the stretch sensor was connected with copper wires to measure the resistivity. As the conventional copper wires provide discomfort to the wearer, stretchable electrodes [59] can be used to connect stretch sensors and data acquisition unit located at less uncomfortable places such as waist.

Acknowledgments

This research was supported by the National Research Foundation (NRF) funded by the Ministry of Science and ICT (MSIT) (NFT-2017M3A9E2063103).

Appendix

The MPI model consists of play and dead-zone operators. Identically, the inverse MPI model also consists of play and dead-zone operators. The only differences relate to the parameters, including weighting constants ($\boldsymbol{w_h}$, $\boldsymbol{w_s}$), thresholds ($\boldsymbol{r_h}$, $\boldsymbol{r_s}$), and initial output values ($\boldsymbol{y_0}$). This is because the inverse MPI model is symmetric with the MPI model. The parameters of the inverse MPI model can be computed analytically using the parameters of the MPI model [56]. The

equations for the transformation are presented below.

$$\mathbf{w'}_h = \begin{cases} w'_{h0} = \dfrac{1}{w_{h0}} \\ w'_{hi} = \dfrac{-w_{hi}}{\left(\sum_{j=0}^{i} w_{hj}\right)\left(\sum_{j=0}^{i-1} w_{hj}\right)}, \; i = 1 \ldots n \end{cases} \tag{A.1}$$

$$\mathbf{w'}_s = \begin{cases} w'_{s0} = \dfrac{1}{w_{s0}} \\ w'_{si} = \dfrac{-w_{hi}}{\left(\sum_{j=0}^{i} w_{sj}\right)\left(\sum_{j=0}^{i-1} w_{sj}\right)}, \; i = 1 \ldots m \end{cases} \tag{A.2}$$

$$r'_{hi} = \sum_{j=0}^{i} w_{hj}(r_{hi} - r_{hj}), i = 1 \ldots n \tag{A.3}$$

$$r'_{si} = \sum_{j=0}^{i} w_{sj}(r_{si} - r_{sj}), i = 1 \ldots m \tag{A.4}$$

$$y'_{0i} = \sum_{j=0}^{i} w_{hj} y_{0i} + \sum_{j=i+1}^{n} w_{hj} y_{0j} \tag{A.5}$$

ORCID iDs

Hyosang Lee https://orcid.org/0000-0001-8984-7870

References

[1] Khan S and Lorenzelli L 2017 Recent advances of conductive nanocomposites in printed and flexible electronics *Smart Mater. Struct.* **26** 083001

[2] Patel S, Park H, Bonato P, Chan L and Rodgers M 2012 A review of wearable sensors and systems with application in rehabilitation *Journal of Neuroengineering and Rehabilitation* **9** 21

[3] Tao W, Liu T, Zheng R and Feng H 2012 Gait analysis using wearable sensors *Sensors* **12** 2255–83

[4] Zhou H, Stone T, Hu H and Harris N 2008 Use of multiple wearable inertial sensors in upper limb motion tracking *Med. Eng. Phys.* **30** 123–33

[5] Yabukami S, Kikuchi H, Yamaguchi M, Arai K, Takahashi K, Itagaki A and Wako N 2000 Motion capture system of magnetic markers using three-axial magnetic field sensor *Magnetics, IEEE Transactions on* **36** 3646–8

[6] Menguc Y, Park Y-L, Martinez-Villalpando E, Aubin P, Zisook M, Stirling L, Wood R J and Walsh C J 2013 Soft wearable motion sensing suit for lower limb biomechanics measurements *Robotics and Automation (ICRA), 2013 IEEE Int. Conf. on* pp 5309–16

[7] Hong J *et al* 2016 A large-strain weft-knitted sensor fabricated by conductive UHMWPE/PANI composite yarns *Sensors and Actuators A: Physical* **238** 307–16

[8] Makikawa M *et al* 2013 Flexible fabric sensor toward a humanoid Robot's skin: fabrication, characterization, and perceptions *IEEE Sens. J.* **13** 4065–80

[9] Cotton D P, Graz I M and Lacour S P 2009 A multifunctional capacitive sensor for stretchable electronic skins *IEEE Sens. J.* **9** 2008–9

[10] Hammock M L, Chortos A, Tee B C-K, Tok J B-H and Bao Z 2013 25th anniversary article: the evolution of electronic skin (E-Skin): a brief history, design considerations, and recent progress *Adv. Mater.* **25** 5997–6038

[11] Cho H, Lee H, Kim Y and Kim J 2017 Design of an optical soft sensor for measuring fingertip force and contact recognition *International Journal of Control, Automation and Systems* **15** 16–24

[12] Truby R L and Lewis J A 2016 Printing soft matter in three dimensions *Nature* **540** 371–8

[13] Yamada T, Hayamizu Y, Yamamoto Y, Yomogida Y, Izadi-Najafabadi A, Futaba D N and Hata K 2011 A stretchable carbon nanotube strain sensor for human-motion detection *Nat. Nanotechnol.* **6** 296–301

[14] Gaikwad A M, Arias A C and Steingart D A 2015 Recent progress on printed flexible batteries: mechanical challenges, printing technologies, and future prospects *Energy Technology* **3** 305–28

[15] Ho C C, Evans J W and Wright P K 2010 Direct write dispenser printing of a zinc microbattery with an ionic liquid gel electrolyte *J. Micromech. Microeng.* **20** 104009

[16] Castano L M and Flatau A B 2014 Smart fabric sensors and e-textile technologies: a review *Smart Mater. Struct.* **23** 053001

[17] Ahmed Z, Torah R and Tudor J 2015 Optimisation of a novel direct-write dispenser printer technique for improving printed smart fabric device performance *Design, Test, Integration and Packaging of MEMS/MOEMS (DTIP), 2015 Symp. on* pp 1–5

[18] Ahmed Z, Torah R, Yang K, Beeby S and Tudor J 2016 Investigation and improvement of the dispenser printing of electrical interconnections for smart fabric applications *Smart Mater. Struct.* **25** 105021

[19] Li Y, Torah R, Beeby S and Tudor J 2015 Fully direct-write dispenser printed dipole antenna on woven polyester cotton fabric for wearable electronics applications *Electron. Lett.* **51** 1306–8

[20] de Vos M, Torah R and Tudor J 2015 A novel pneumatic dispenser fabrication technique for digitally printing electroluminescent lamps on fabric *Design, Test, Integration and Packaging of MEMS/MOEMS (DTIP), 2015 Symp. on* pp 1–4

[21] Whittow W G, Chauraya A, Vardaxoglou J, Li Y, Torah R, Yang K, Beeby S and Tudor J 2014 Inkjet-printed microstrip patch antennas realized on textile for wearable applications *IEEE Antennas and Wireless Propagation Letters* **13** 71–4

[22] Amjadi M, Yoon Y J and Park I 2015 Ultra-stretchable and skin-mountable strain sensors using carbon nanotubes? Ecoflex nanocomposites *Nanotechnology* **26** 375501

[23] Gibbs P T and Asada H H 2005 Wearable conductive fiber sensors for multi-axis human joint angle measurements *Journal of NeuroEngineering and Rehabilitation* **2** 7

[24] Kappel S L, Rathleff M S, Hermann D, Simonsen O, Karstoft H and Ahrendt P 2012 A novel method for measuring in-shoe navicular drop during gait *Sensors* **12** 11697–711

[25] Tognetti A, Carbonaro N, Zupone G and De Rossi D 2006 Characterization of a novel data glove based on textile integrated sensors *Engineering in Medicine and Biology Society, 2006. EMBS'06. 28th Annual Int. Conf. of the IEEE* pp 2510–3

[26] Lu N, Lu C, Yang S and Rogers J 2012 Highly sensitive skin-mountable strain gauges based entirely on elastomers *Adv. Funct. Mater.* **22** 4044–50

[27] Wang Y, Wang L, Yang T, Li X, Zang X, Zhu M, Wang K, Wu D and Zhu H 2014 Wearable and highly sensitive graphene strain sensors for human motion monitoring *Adv. Funct. Mater.* **24** 4666–70
[28] Lorussi F, Galatolo S, Bartalesi R and De Rossi D 2013 Modeling and characterization of extensible wearable textile-based electrogoniometers *Sensors Journal, IEEE* **13** 217–28
[29] Lorussi F, Scilingo E P, Tesconi M, Tognetti A and De Rossi D 2005 Strain sensing fabric for hand posture and gesture monitoring *IEEE Transactions on Information Technology in Biomedicine* **9** 372–81
[30] Pacelli M, Caldani L and Paradiso R 2006 Textile piezoresistive sensors for biomechanical variables monitoring *Engineering in Medicine and Biology Society, 2006. EMBS'06. 28th Annual Int. Conf. of the IEEE* pp 5358–61
[31] Obitayo W and Liu T 2012 A review: Carbon nanotube-based piezoresistive strain sensors *Journal of Sensors* **2012** 652438
[32] Bouhamed A, Müller C, Choura S and Kanoun O 2017 Processing and characterization of MWCNTs/epoxy nanocomposites thin films for strain sensing applications *Sensors and Actuators A: Physical* **257** 65–72
[33] Lee H, Kwon D, Cho H, Park I and Kim J 2017 Soft nanocomposite based multi-point, multi-directional strain mapping sensor using anisotropic electrical impedance tomography *Sci. Rep.* **7** 39837
[34] Sanli A, Benchirouf A, Müller C and Kanoun O 2017 Piezoresistive performance characterization of strain sensitive multi-walled carbon nanotube-epoxy nanocomposites *Sensors and Actuators A: Physical* **254** 61–8
[35] Lee J, Kim S, Lee J, Yang D, Park B C, Ryu S and Park I 2014 A stretchable strain sensor based on a metal nanoparticle thin film for human motion detection *Nanoscale* **6** 11932–9
[36] Amjadi M, Pichitpajongkit A, Lee S, Ryu S and Park I 2014 Highly stretchable and sensitive strain sensor based on silver nanowire–elastomer nanocomposite *ACS Nano* **8** 5154–63
[37] Kinloch A 2012 *Adhesion and Adhesives: Science and Technology* (Netherlands: Springer)
[38] Jia Y, Jiang Z, Peng J, Gong X and Zhang Z 2012 Resistance to time-dependent deformation of polystyrene/carbon nanotube composites under cyclic tension *Composites Part A: Applied Science and Manufacturing* **43** 1561–8
[39] Lozano-Perez C, Cauich-Rodriguez J and Aviles F 2016 Influence of rigid segment and carbon nanotube concentration on the cyclic piezoresistive and hysteretic behavior of multiwall carbon nanotube/segmented polyurethane composites *Compos. Sci. Technol.* **128** 25–32
[40] Wang L, Han Y, Wu C and Huang Y 2013 A solution to reduce the time dependence of the output resistance of a viscoelastic and piezoresistive element *Smart Mater. Struct.* **22** 075021
[41] Kim J-S and Kim G-W 2017 Hysteresis compensation of piezoresistive carbon nanotube/polydimethylsiloxane composite-based force sensors *Sensors* **17** 229
[42] Sánchez-Durán J A, Oballe-Peinado Ó, Castellanos-Ramos J and Vidal-Verdú F 2012 Hysteresis correction of tactile sensor response with a generalized Prandtl–Ishlinskii model *Microsyst. Technol.* **18** 1127–38
[43] Bokobza L 2007 Multiwall carbon nanotube elastomeric composites: a review *Polymer* **48** 4907–20
[44] Ponnamma D, Sadasivuni K K, Grohens Y, Guo Q and Thomas S 2014 Carbon nanotube based elastomer composites–an approach towards multifunctional materials *J. Mater. Chem.* C **2** 8446–85
[45] Stauffer D and Aharony A 1994 *Introduction to Percolation Theory* (Boca Raton, FL: CRC press)
[46] Lee H, Cho J and Kim J 2016 Printable skin adhesive stretch sensor for measuring multi-axis human joint angles *Robotics and Automation (ICRA), 2016 IEEE Int. Conf. on* pp 4975–80
[47] ASTM 2015 *Standard test method for peel resistance of adhesives (T-peel test)* D1876-08(2015)e1 (https://doi.org/10.1520/D1876-08R15E01)
[48] Dally J W, Riley W F and Kobayashi A 1978 Experimental stress analysis *Journal of Applied Mechanics* **45** 968
[49] Wang L and Li Y 2013 A review for conductive polymer piezoresistive composites and a development of a compliant pressure transducer *Instrumentation and Measurement, IEEE Transactions on* **62** 495–502
[50] Yang L, Ge Y, Zhu Q, Zhang C, Wang Z and Liu P 2012 Experimental and numerical studies on the sensitivity of carbon fibre/silicone rubber composite sensors *Smart Mater. Struct.* **21** 035011
[51] Bao W, Meguid S, Zhu Z and Weng G 2012 Tunneling resistance and its effect on the electrical conductivity of carbon nanotube nanocomposites *J. Appl. Phys.* **111** 093726
[52] Lv Y, Guo L, Wang Y and Deng Z 2016 Tension behavior of filled silicone rubbers at different temperatures *Advanced Materials, Mechanical and Structural Engineering: Proc. of the 2nd Int. Conf. of Advanced Materials, Mechanical and Structural Engineering (AMMSE 2015) (Je-ju Island, South Korea, September 18–20, 2015)* p 91
[53] Rey T, Chagnon G, Le Cam J-B and Favier D 2013 Effects of temperature on the mechanical behavior of filled and unfilled silicone rubbers *8th European Conf. on Constitutive Models for Rubbers* pp 511–4
[54] Oskouyi A B, Sundararaj U and Mertiny P 2014 Effect of temperature on electrical resistivity of carbon nanotubes and graphene nanoplatelets nanocomposites *Journal of Nanotechnology in Engineering and Medicine* **5** 044501
[55] Mayergoyz I D 2003 *Mathematical Models of Hysteresis and Their Applications* (United States: Elsevier)
[56] Kuhnen K 2003 Modeling, identification and compensation of complex hysteretic nonlinearities: a modified Prandtl-Ishlinskii approach *Eur. J. Control* **9** 407–18
[57] McNally T and Pötschke P 2011 *Polymer-Carbon Nanotube Composites: Preparation, Properties and Applications* (Amsterdam: Elsevier)
[58] Chossat J-B, Park Y-L, Wood R J and Duchaine V 2013 A soft strain sensor based on ionic and metal liquids *IEEE Sens. J.* **13** 3405–14
[59] Lu N and Kim D-H 2014 Flexible and stretchable electronics paving the way for soft robotics *Soft Robotics* **1** 53–62